

Article

Ultrasound-Assisted Hydrothermal Synthesis of V₂O₅/Zr-SBA-15 Catalysts for Production of Ultralow Sulfur Fuel

Jesús Miguel Ramos ¹, Jin An Wang ^{1,*} , Sergio Odin Flores ¹, Lifang Chen ¹, Ulises Arellano ² , Luis Enrique Noreña ³, Julio González ⁴  and Juan Navarrete ⁵

- ¹ Escuela Superior de Ingeniería Química e Industrias Extractivas, Instituto Politécnico Nacional, Av. Instituto Politécnico Nacional s/n, Col. Zacatenco, Ciudad de México 07738, Mexico; jesus_miguel_rc@hotmail.com (J.M.R.); sergiodin@gmail.com (S.O.F.); lchen@ipn.mx (L.C.)
- ² Departamento de Química, Universidad Autónoma Metropolitana-Iztapalapa, Av. San Rafael Atlixco No. 186, Ciudad de México 09340, Mexico; lukas261100@hotmail.com
- ³ Departamento de Ciencias Básicas, Universidad Autónoma Metropolitana-Azcapotzalco, Av. San Pablo 180, Ciudad de México 02200, Mexico; lnf@azc.uam.mx
- ⁴ Tecnológico de Estudios Superiores de Coacalco, Av. 16 de Septiembre No. 54, Col. Cabecera Municipal, Coacalco de Berriozabal, Estado de México 55700, Mexico; jgon88@hotmail.com
- ⁵ Dirección de Investigación, Instituto Mexicano del Petróleo, Eje Lázaro Cárdenas No. 152, Ciudad de México 07730, Mexico; jnavarre@imp.mx
- * Correspondence: jwang@ipn.mx



Citation: Ramos, J.M.; Wang, J.A.; Flores, S.O.; Chen, L.; Arellano, U.; Noreña, L.E.; González, J.; Navarrete, J. Ultrasound-Assisted Hydrothermal Synthesis of V₂O₅/Zr-SBA-15 Catalysts for Production of Ultralow Sulfur Fuel. *Catalysts* **2021**, *11*, 408. <https://doi.org/10.3390/catal11040408>

Academic Editors: Prince Nana Amaniampong and Sabine Valange

Received: 22 February 2021
Accepted: 18 March 2021
Published: 24 March 2021

Publisher's Note: MDPI stays neutral with regard to jurisdictional claims in published maps and institutional affiliations.



Copyright: © 2021 by the authors. Licensee MDPI, Basel, Switzerland. This article is an open access article distributed under the terms and conditions of the Creative Commons Attribution (CC BY) license (<https://creativecommons.org/licenses/by/4.0/>).

Abstract: This work reports the results of the ultrasound-assisted hydrothermal synthesis of two sets of V₂O₅ dispersed on SBA-15 and Zr doped SBA-15 catalysts used for the oxidation of dibenzothiophene (DBT) in a model diesel via the combination of oxidation, catalysis, and extraction technical route. These catalysts contained Lewis acidity as major and Brønsted acidity as minor. The amount of acidity varied with the content of vanadia and zirconium doping. It was found that DBT conversion is very sensitive to the Lewis acidity. DBT conversion increased by increasing the vanadium content and correlated well with the amount of surface Lewis acidity. Under the optimal experimental condition (Reaction temperature: 60 °C, reaction time 40 min, catalyst concentration: 1 g/L oil; H₂O₂/DBT mole ratio = 10), the 30% V₂O₅/SBA-15 and 30% V₂O₅/Zr-SBA-15 catalysts could convert more than 99% of DBT. Two reaction pathways of DBT oxidation involving vanadia surface structure, Lewis acidity, and peroxometallic complexes were proposed. When the vanadia loading V₂O₅ ≤ 10 wt%, the oxidative desulfurization (ODS) went through the Pathway I; in the catalysts with moderate vanadia content (V₂O₅ = 20–30 wt%), ODS proceeded via the Pathways II or/and the Pathway I.

Keywords: clean fuel; surface acidity; vanadia; dibenzothiophene

1. Introduction

It is well known that petroleum contains a wide spectrum of organosulfur compounds such as disulfides, thiophene, dibenzothiophene (DBT), and their alkylated derivatives [1]. These sulfur-containing compounds must be removed before the fluid catalytic cracking (FCC) process to avoid the release of a heavy amount of SO_x emissions. The traditional hydrodesulfurization (HDS) technology has been applied in the oil refining industry for petroleum hydrotreating and sulfur removal [1,2]. However, HDS process is efficient only for diminishing sulfur concentration from thousands ppm to approximately hundreds ppm at a reasonable cost [2–4]. Most sulfur residuals retaining in the hydrotreated oil are the refractory polyaromatic sulfur compounds due to their steric hindrance and higher resistance to hydrodesulfurization [5,6]. Therefore, hydrotreated petroleum products such as gasoline or diesel usually contain a certain amount of organosulfur compounds. For further reducing their concentration from hundred ppm to ultralow sulfur concentration in order to meet

the increasingly strict environment regulations, the operation parameters of the existing HDS process must be properly modified. For example, the reaction temperature, H₂ to oil ratio, and catalyst load have to be increased [7,8]. All these modifications lead to a higher total operation cost. Other alternative technologies, including bio-desulfurization [9–13], oxidative desulfurization (ODS) [14–16], adsorption and extraction [17–21] and so forth, have been investigated for the production of fuels with ultralow sulfur content. Amongst these, the ODS technology has attracted considerable attention because of several advantages over HDS: (i) operation at a temperature lower than 100 °C under atmospheric pressure; (ii) no expensive hydrogen consumption; (iii) higher efficiency for the removal of refractory polyaromatic sulfur compounds; and (iv) approximately 10–20% reduction of the total cost with respect to the modified HDS technique [8].

In the oxidative desulfurization, the sulfur compounds are converted to corresponding sulfones which can be removed by the following steps such as extraction, adsorption, distillation, and others. Generally, for sulfur oxidation, both oxidant and heterogeneous catalyst take the key roles. Hydrogen peroxide [22,23], organic peroxides [24], tert-butyl hydroperoxide (TBHP) [25], molecular oxygen [26], and others have been reported as effective oxidation agents. Of these oxidants, H₂O₂ is mostly used due to its availability, environmentally friendly character, and its high oxidation potential.

Many investigations have focused on ionic liquids, soluble metal complexes and transition metal oxides as catalysts for ODS reactions. The application of ionic liquids for sulfur removal has been extensively examined [27–32]. However, the high price, and residual of a part of ionic liquids in fuel are the main drawbacks. Al Shahrani et al. [27] reported a simplified ODS catalytic system using soluble Na₂WO₄ as catalyst for deep removal of sulfur from diesel. It can diminish sulfur concentration from 1100 ppm to 40 ppm in a real diesel fuel and reach 100% conversion of thiophenes to sulfones for a model fuel. Unfortunately, the re-utilization and separation of the homogeneous catalysts stand as the major challenges. To overcome these limitations, heterogeneous solid catalysts such as transition metal oxides with higher chemical oxidation states dispersed on different supports have been widely studied. Transition metal oxides such as Mo(VI) [33–35], W(VI) [36,37], V(V) [38–40], Ti(IV) [41,42], and Fe(III) [43] oxides are reported to be active for ODS reactions.

In the design of heterogeneous solid catalysts, metal oxides such as Al₂O₃, SiO₂, TiO₂, CeO₂, Nb₂O₅, ZrO₂, and hydrotalcite-like solids have been applied as support used for ODS reaction [39,44–46]. Activated carbon materials are widely applied as both adsorbent and catalyst support in the ODS process [21,47–49]. Because the cross-cutting molecular size of polyaromatic sulfur compounds is relatively large, for instance, the topological polar surface area of 4,6-dimethyldibenzothiophene (4,6-DMDBT) is approximately 28.2 Å², the diffusion of both 4,6-DMDBT and corresponding 4,6-DMDBTO₂ sulfone product across pores of the catalyst definitely affects the catalytic efficiency. Therefore, the catalyst support used for ODS reaction must possess big pore size and large surface area. It is reported that mesoporous SAPO-11 with various crystalline MoO₃ phases [50] and large-pore silica as catalyst supports for samarium-coordinated undecamolybdophosphate were effective for ODS of diesel [51]. Zhu et al. claimed that 3D-printing of integrated spheres can be used as a superior support of phosphotungstic acid for deep oxidative desulfurization of fuel [52].

Some mesoporous materials, like MCM-41 and SBA-15, have been investigated as catalyst support due to their proper textural properties and good thermal stability. González et al. reported that VO_x/Ti-MCM-41 catalysts for DBT oxidation, 99.9% of DBT could be removed from a model diesel using a 25 wt%V₂O₅/Ti-MCM-41 catalyst under the optimal operation condition [38]. Ti-MCM-41 supported vanadia core-shell catalysts were also reported for simultaneous oxidation of refractory DBT, 4-methyldibenzothiophene (4-MDBT) and 4,6-dimethyldibenzothiophene (4,6-DMDBT) in a model diesel fuel, achieving high ODS efficiency [40]. WO₃ and MoO₃ supported on SBA-15 were reported to be very active for 4,6-DMDBT oxidation [33,37]. Al-SBA-15 modified with molybdenum oxide

and Anderson-type polyoxometalate (POM) catalysts used for DBT oxidation were also reported [53,54].

It is noteworthy that selection of a proper preparation method and starting chemical precursors influence on the price of the final catalyst. For example, although WO_3 and MoO_3 supported on SBA-15 catalysts were very active for 4,6-DMDBT oxidation [33,37], they are more expensive in comparison with vanadia supported catalysts due to their more expensive W and Mo precursors. Moreover, the surface acidity of the heterogeneous catalysts usually take important roles in the adsorption of sulfur compounds and surface reactions during the ODS procedure [33,37,38]. Investigation on the influence of surface acidity on the sulfur oxidation in the ODS reaction is still an interesting topic.

In this work, an ultrasound-assisted hydrothermal synthesis of highly active vanadia dispersed on mesoporous SBA-15 catalysts is reported with the purpose of shortening the synthesis time and lowering the cost of the catalysts. Particular attention was paid to the influence of the Lewis acidity of the catalysts on the ODS activity, aiming at establishing a possible quantitative correlation of surface acidity with the catalyst activity. ODS mechanisms involving vanadia nanoclusters, surface Lewis acid sites, and formation of peroxometallic complexes are proposed. With the designed ODS reaction system reported herein, the oxidation of organosulfurs and the separation of resultant sulfones can be operated in one operation unit.

2. Results and Discussion

2.1. X-ray Diffraction Characterization

Figure 1A shows the X-ray diffraction diagrams of $\text{V}_2\text{O}_5/\text{SBA-15}$ catalysts with different V_2O_5 loading (The obtained catalysts termed as nV/SBA-15 and nV/Zr-SBA-15 in tables and figures; sometimes, they are also written as n wt% $\text{V}_2\text{O}_5/\text{SBA-15}$ or n $\text{V}_2\text{O}_5/\text{Zr-SBA-15}$, where n indicates the V_2O_5 loading at weight percentage). For all the three catalysts, there was one wide and strong peak at 2θ between 16° and 30° which resulted from the amorphous silica phase, herein the SBA-15 support. For the 10 wt% $\text{V}_2\text{O}_5/\text{SBA-15}$, the weak XRD peaks appeared at 2θ of $15.2, 20.4, 26.8, 31.7, 32.3,$ and 34.5° , corresponding to the (200), (001), (101), (110), (301), (011) planes of V_2O_5 crystals with orthorhombic crystalline structure (Joint Committee on Powder Diffraction Standards (JCPDS) No. 19-387). XRD patterns indicate the high dispersion of vanadia nanoparticles in this sample. When the vanadia content increased, the peak intensity corresponding to V_2O_5 increased, and more peaks at 2θ of $41.0, 46.3, 47.3, 51.5, 56.0, 57.8, 62.0,$ and 67.3° appeared, corresponding to (310), (002), (600), (012), (412), (710), (711), and (413) planes of V_2O_5 crystals with orthorhombic crystalline structure (JCPDS No. 19-387). For the 30 wt% $\text{V}_2\text{O}_5/\text{SBA-15}$ catalyst, the diffraction peaks became sharper and stronger, indicating that the crystallite size of vanadia became larger. The lattice cell parameters of the orthorhombic V_2O_5 crystal are $a = 11.51 \text{ \AA}$, $b = 3.56 \text{ \AA}$, and $c = 4.36 \text{ \AA}$. The XRD patterns of $\text{V}_2\text{O}_5/\text{Zr-SBA-15}$ catalysts, Figure 1B, are very similar to that shown for the $\text{V}_2\text{O}_5/\text{SBA-15}$ samples. However, for the 30 wt% $\text{V}_2\text{O}_5/\text{Zr-SBA-15}$, two small peaks at 2θ of 26.0° and 29.6° appeared; they are assigned to the crystalline phase of tetragonal zirconia ($t\text{-ZrO}_2$). A small amount of zirconium segregated from the SBA-15 solid, forming the $t\text{-ZrO}_2$ phase during the reaction and calcination procedure.

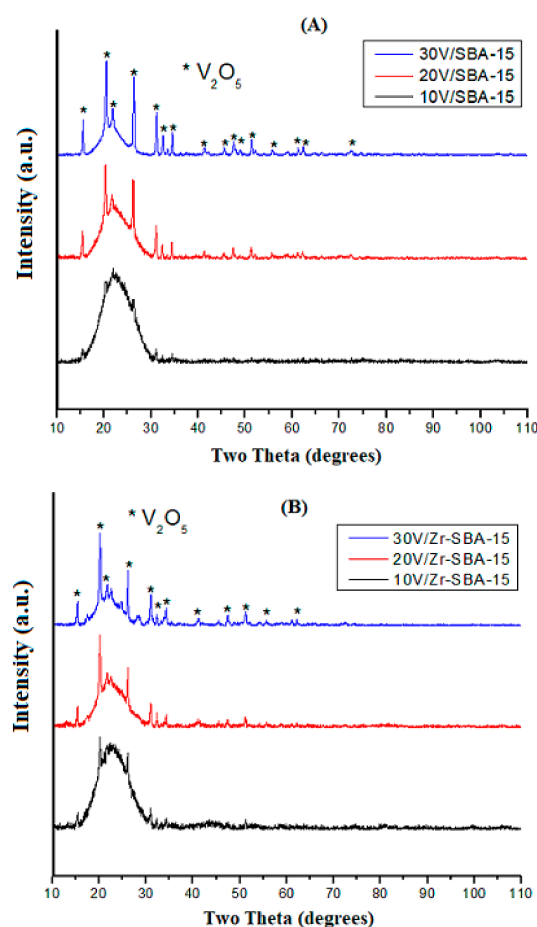


Figure 1. XRD spectra of catalysts (A) SBA-15 and V_2O_5 /SBA-15; (B) Zr-SBA-15 and V_2O_5 /Zr-SBA-15.

2.2. Textural Properties— N_2 -Physisorption Isotherms

The textural properties of the support and vanadia loaded catalysts were measured by the N_2 adsorption-desorption isotherm method. The pure SBA-15 solid, Figure 2a, showed features corresponding to type IV isotherms [55]. The hysteresis loop in the P/P_0 range from 0.4 to 0.85 indicated N_2 capillary condensation in mesopores. For the V_2O_5 /SBA-15 samples, the shape of the hysteresis loop largely remained unchanged even after loading 30 wt% of V_2O_5 , confirming that the pore structure of the parent material was preserved. However, the adsorbed volume diminished; therefore, the porosity was lost to some degree.

The Zr doped SBA-15 showed the N_2 adsorption-desorption curve is very similar to that observed for the SBA-15 solid (Figure 2b). These results confirmed that the mesoporous structure of Zr-SBA-15 remained unchanged after zirconium doping. When V_2O_5 was deposited on the surface of SBA-15 or Zr-SBA-15, the pore volume dramatically decreased (Table 1).

For the V_2O_5 /SBA-15 and V_2O_5 /Zr-SBA-15 catalysts, vanadia deposition led to a decrease of surface area that was probably caused by the incorporation of V_2O_5 inside the mesopores. It is noteworthy that for the 30 wt% V_2O_5 /SBA-15, the surface area significantly diminished to $114 \text{ m}^2/\text{g}$ and the average pore size increased to 17.5 nm. This should be related to the collapse of the walls between the adjacent pores at higher vanadium content after calcination. Three adjacent pores merged into a large pore with diameter approximately 16~18 nm. However, the pore collapse phenomenon was not observed for the 30 wt% V_2O_5 /Zr-SBA-15 samples. Therefore, Zr doping SBA-15 improves the texture or structure stability of the catalysts.

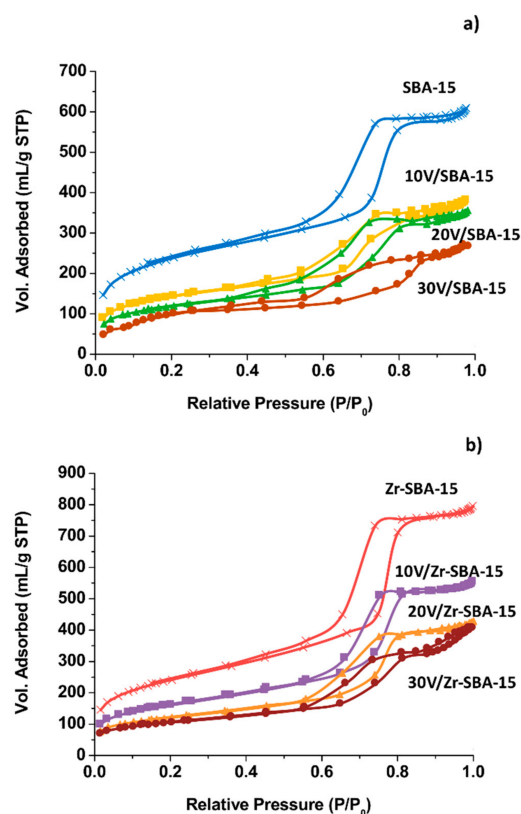


Figure 2. Features of nitrogen adsorption-desorption isotherms. (a) SBA-15 and V₂O₅/SBA-15; (b) Zr-SBA-15 and V₂O₅/Zr-SBA-15.

Table 1. Porosity and pore wall thickness of the SBA-15, Zr-SBA-15, V₂O₅/SBA-15, and V₂O₅/Zr-SBA-15 catalysts.

Sample	SA (m ² /g)	D _p (nm)	V _p (cm ³ /g)	W(nm)
SBA-15	873	5.2	0.93	4.8
10V/SBA-15	509	5.1	0.59	4.9
20V/SBA-15	415	5.6	0.58	4.4
30V/SBA-15	114	17.5	0.41	4.3
Zr-SBA-15	910	5.7	1.39	4.4
10V/Zr-SBA-15	580	5.8	0.95	4.3
20V/Zr-SBA-15	412	5.8	0.72	4.3
30V/Zr-SBA-15	341	6.8	0.70	4.4

SA: surface area obtained from the Brunauer-Emmett-Teller (BET) model; V_p: pore volume; D_p: average pore diameter; W: pore wall thickness ($W = a_0 - D_{\text{BJH}}$) where a_0 is lattice cell parameter and D_{BJH} is pore diameter obtained from the Barrett-Joyner-Halenda (BJH) model of N₂ adsorption isotherm.

2.3. Surface Acidity Measurement

The surface acidity of supports and catalysts was measured by using in situ pyridine adsorption FTIR technique. To eliminate the effect of any trace of physisorption of pyridine on the samples, all the IR spectra recorded at 100 °C under vacuum condition were used for the acid data calculation (not shown). Surface Lewis centers (terms L) were indicated by several characteristic IR bands at 1444 cm⁻¹, 1595 cm⁻¹, and 1603 cm⁻¹; while the Brønsted acid centers were characterized by IR peak at around 1541 cm⁻¹ (terms B) [33,56]. The band at around 1489 cm⁻¹ was reported to the pyridine molecule associating with the neighboring L and B centers (noted as L+B) [33,56]. For the six catalysts, the density of Lewis acidity was much greater than the Brønsted acidity. The intensity of the IR band related to Lewis acidity gradually increased by increasing the vanadia content. Both SBA-

15 and Zr-SBA-15 supports contained mainly Lewis acid centers. However, Zr-SBA-15 showed stronger IR bands than SBA-15, indicating that Zr doping created additional acid sites in the SBA-15 solid.

Table 2 shows the quantitative acid data. Zr doping led to an increment of the total acidity of pure SBA-15 by approximately 25%. Vanadium loading greatly affects the surface acidity of the catalysts. For instance, for V_2O_5 /SBA-15 catalysts, relative to bare SBA-15, the total acidity increased by 37.9%, 54.8% and 75.5% as the vanadia content was increased from 10 wt% to 20 and 30 wt%, respectively. For the V_2O_5 /Zr-SBA-15 catalysts, vanadia loading led to the total acidity increasing by 49.7% (for 10 wt% V_2O_5), 69.9% (for 20 wt% V_2O_5), and 100.7% (for 30 wt% V_2O_5) with respect to the Zr-SBA-15 support. Brønsted acidity decreases at increasing of vanadia loading in the V_2O_5 /Zr-SBA-15 catalysts. Both vanadia loading and zirconium doping are chiefly responsible for the creation of new Lewis acid sites.

Table 2. Surface acidity data of SBA-15, Zr-SBA-15, V_2O_5 /SBA-15, and V_2O_5 /Zr-SBA-15 catalysts.

Sample	Brønsted ($\mu\text{moles/g}$)	Lewis ($\mu\text{moles/g}$)	Total Acidity ($\mu\text{moles/g}$)
SBA-15	46	851	897
10V/SBA-15	39	1198	1237
20V/SBA-15	73	1314	1387
30V/SBA-15	61	1513	1574
Zr-SBA-15	62	1057	1119
10V/Zr-SBA-15	73	1602	1675
20V/Zr-SBA-15	17	1884	1901
30V/Zr-SBA-15	14	2232	2246

2.4. Morphological Features—SEM and TEM Observations

The V_2O_5 /SBA-15 catalysts showed a fibrous chain-like morphology (Figure 3). The solids were composed of rods interconnected particles forming fibers. The length of these fibers was in tens of micrometers or greater and they interlaced together. For the sample with higher vanadia content, i.e., 30% V_2O_5 /SBA-15, the fibers were relatively shorter, and they were obviously disordered in comparison with the other two samples. Similar morphologies were observed for the V_2O_5 /Zr-SBA-15 catalysts (Figure 4).

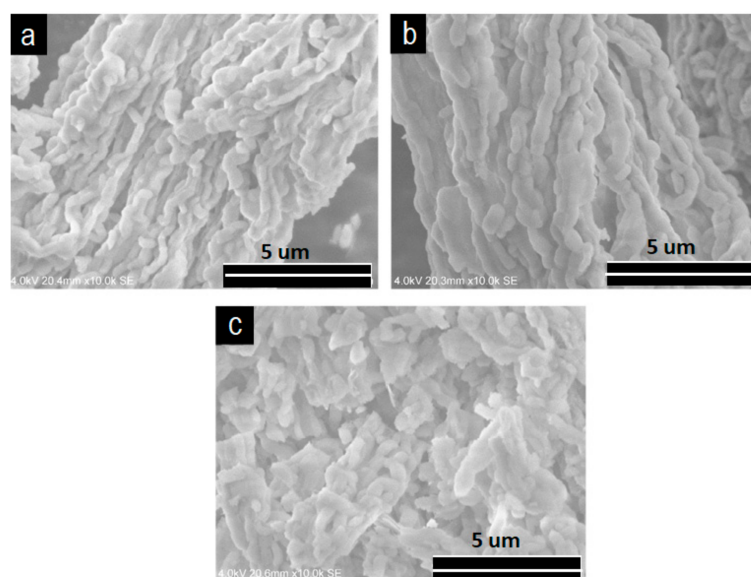


Figure 3. SEM images of V_2O_5 /SBA-15. (A) 10V/SBA-15; (B) 20V/SBA-15; (C) 30V/SBA-15.

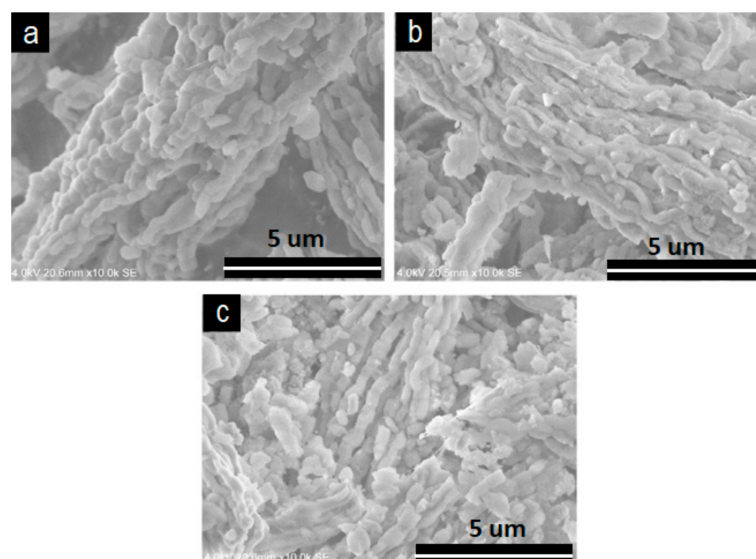


Figure 4. SEM images of $V_2O_5/Zr-SBA-15$. (A) 10V/ $Zr-SBA-15$; (B) 20V/ $Zr-SBA-15$; (C) 30V/ $Zr-SBA-15$.

Figure 5 shows the TEM images of various samples from which morphological features and vanadia particle size distributions on the support are observed. For the SBA-15 solid, Figure 5A, well ordered parallel channels are shown. Figure 5B shows the ordered mesopores with hexagonal arrangements for the Zr doped support. Figure 5C–F show the vanadia deposited catalysts where vanadia particles are well dispersed on the surface of supports. Some small particles are anchored into pore walls or inside mesopores. For the catalysts with higher vanadia loading, i.e., 30 wt% / $Zr-SBA-15$ (Figure 5F), vanadia particles with size approximately 10–20 nm gathered into agglomerates (50–100 nm) on the surface.

2.5. Surface Species Analysis—Raman Spectroscopy

Micro Raman spectroscopy is a sensitive technique for surface metal-oxygen bond characterization. Generally, the Raman band around 990 cm^{-1} corresponds to the stretching vibration of vanadyl $V=O$ bonds and a number of such bonds in this region indicates the number of nonequivalent vanadyl bonds. In our catalysts, Figure 6, two bands at around 1033 and 992 cm^{-1} correspond to the symmetric stretching vibration of terminal oxygen ($V=O$) in vanadyl modes; these oxygen atoms are not shared by VO_4 pyramids [57]. The appearance of these two bands in this region indicates the formation of the $\beta-V_2O_5$ phase, which differs from the only one band at approximately 996 cm^{-1} corresponding to the $\nu(d1)$ mode in the Raman spectrum of the $\alpha-V_2O_5$ phase [57–59].

The bands at 699 and 406 cm^{-1} are attributed to the stretching vibration mode of V doubly coordinated oxygen (V_2-O) in the shared corners [57]. The band at 699 cm^{-1} also indicates the presence of the $\alpha-V_2O_5$ structure. The small band at around 530 cm^{-1} is assigned to triply coordinated oxygen atoms that link three VO_4 pyramids (shared edges). The sharp band at 143 cm^{-1} corresponds to the rigid layer-like mode of the lattice vibrations of $-O-V-O-V-O-$ in the crystalline structure of V_2O_5 and involved at least two basic units of V_2O_5 . The intensity of this band was much stronger than all the other vibration modes, indicating the presence of V_2O_5 microcrystals [38]. The intensity of the Raman bands varying with the V_2O_5 loading indicates the formation of more polymeric V_2O_5 crystals. Raman spectroscopic characterization confirms that two phases ($\alpha-V_2O_5$ and $\beta-V_2O_5$) coexisted and various surface vanadium oxygen bonds (V_3-O , V_2-O , $V-O$, and $V=O$) in the crystalline structure of $\alpha-V_2O_5$ and $\beta-V_2O_5$ phases were present on the surface of catalysts.

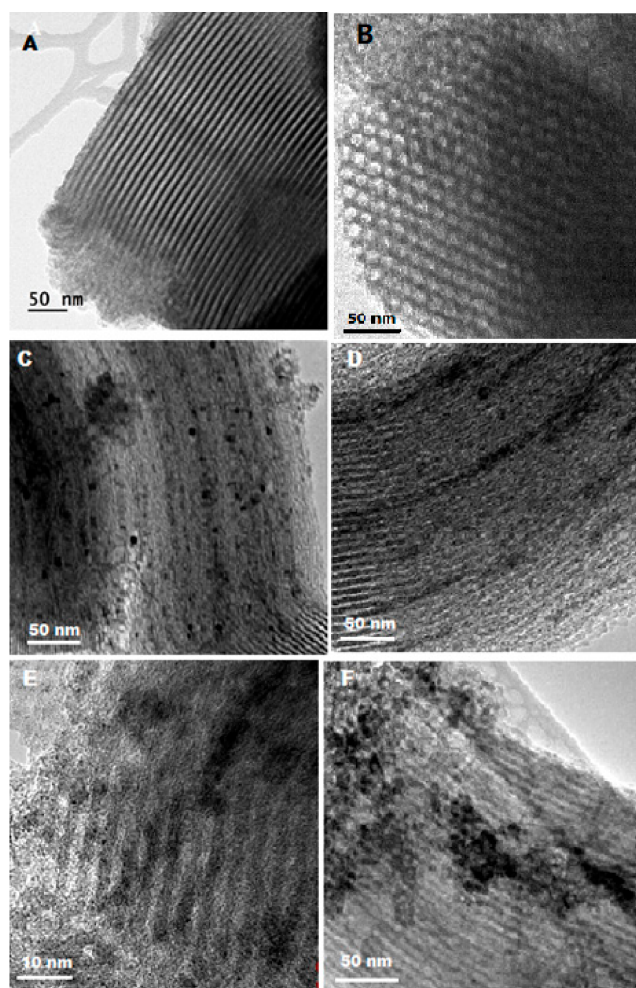


Figure 5. TEM micrographs. (A) BA-15; (B) Zr-SBA-15; (C) 30 V/SBA-15; (D) 10V/SBA-15; (E) 10 V/Zr-SBA-15; (F) 30V/Zr-SBA-15.

2.6. Catalytic Properties—Dibenzothiophene Oxidation and Removal

2.6.1. Effect of H_2O_2 /DBT Molar Ratio (R)

The effect of the R value on the oxidation of DBT was evaluated at a condition based on our previous experience (reaction temperature: 50 °C; catalyst dosage: 1 g/L oil; reaction time: 60 min; volume ratio of oil to acetonitrile 1:1). Figure 7 shows the results of DBT oxidative removal over 20 wt% V_2O_5 /Zr-SBA-15 at R values varying from 2 to 5, 10 and 15. Only one oxygen atom in each H_2O_2 molecule participates in the oxidation of the sulfur atom in DBT and the other O atom joins into water molecule as by-product. When the R value was 2, that is the theoretical stoichiometric value for the DBT complete oxidation, the DBT conversion was lower than 65% after 60 min of reaction. As the R value increased to 5, the DBT conversion was enhanced to 87.5%. The ODS activity significantly increased to 98.6% at R = 10. For R = 15, the catalyst showed DBT conversion greater than 99%, slightly better than that achieved with R of 10. Theoretically, when R value was 2, hydrogen peroxide should provide sufficient oxygen to convert all the DBT into sulfone. However, the actual experiments showed that a stoichiometric hydrogen peroxide was not enough for the complete desulfurization, presumably because of the fact that some active oxygen is located at an unfavorable position for DBT oxidation and they did not participate in the ODS reaction. For the other catalysts, the best ODS results were also obtained at R value 10. In our following experiments, R value was fixed at 10.

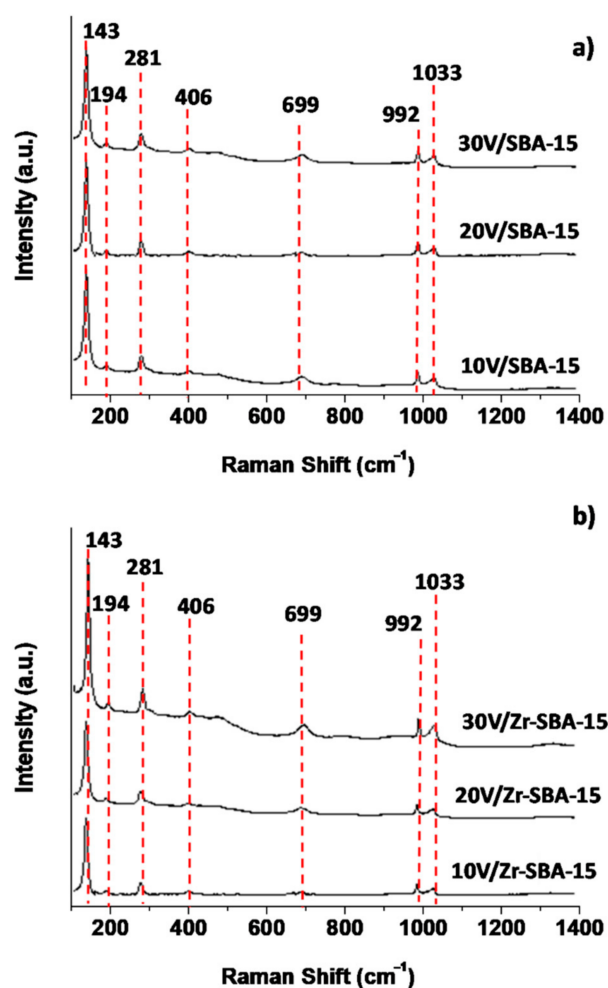


Figure 6. Raman spectra. (a) $V_2O_5/SBA-15$; (b) $V_2O_5/Zr-SBA-15$.

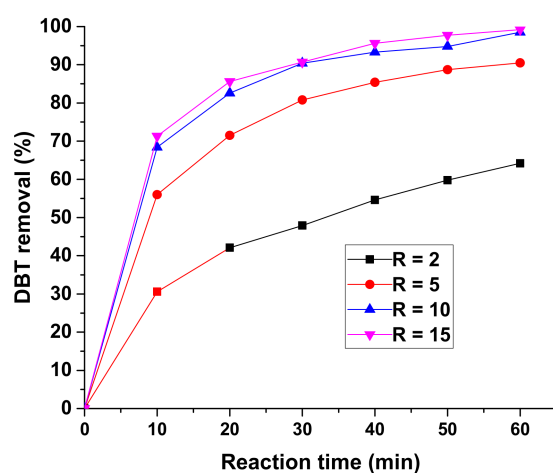


Figure 7. Effect of H_2O_2 /dibenzothiophene (DBT) molar ratio on the 20 wt% $V_2O_5/Zr-SBA-15$. Reaction conditions: catalyst loading: 1 g/L oil; reaction temperature: 50 °C; reaction time: 60 min; oil/acetonitrile volume ratio: 1:1.

2.6.2. Effect of Reaction Temperature

The DBT oxidation was explored at 40, 60, 80, and 100 °C but keeping in the other parameters the same as that reported above (R = 10, catalyst dosage: 1 g/L oil; reaction time: 60 min, volume ratio of oil to acetonitrile 1:1). The results are shown in Figure 8.

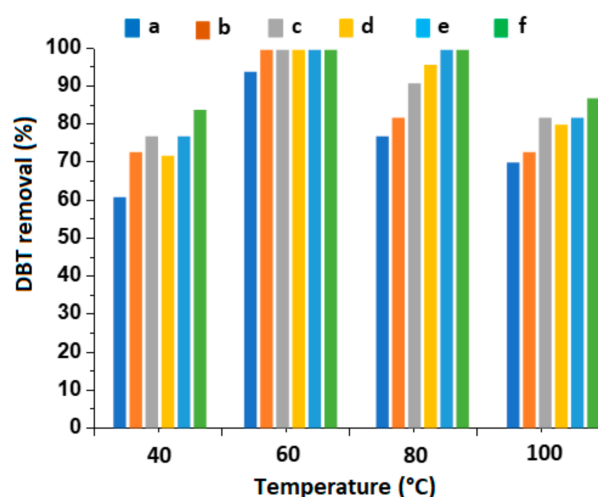


Figure 8. DBT removal at different reaction temperatures. Reaction condition: catalyst loading: 1 g/L oil; H_2O_2 /DBT molar ratio: 10; reaction time: 60 min; oil/acetonitrile volume ratio: 1:1. (a) 10V/SBA-15; (b) 20V/SBA-15; (c) 30V/SBA-15; (d) 10V/Zr-SBA-15; (e) 20V/Zr-SBA-15; (f) 30V/Zr-SBA-15.

At a lower reaction temperature, i.e., 40 °C, DBT conversion varied between 61.6 and 84.5% on different catalysts. When the temperature increased to 60 °C, the DBT oxidation was significantly increased, near completion for both sets of catalysts, except for the 10% V_2O_5 /SBA-15 where DBT conversion was 94.3%. At 80 °C, the DBT oxidation was slightly decreased for the catalysts with 10 and 20 wt% vanadia. At 100 °C, the DBT conversion was dramatically diminished to less than 88.6%. At lower temperature (40 °C), the interaction of the catalyst with H_2O_2 and DBT molecules was relatively weak, the catalysts were not activated enough for sulfur oxidation, and thus they exhibited lower catalytic activity. Therefore, complete oxidation of DBT was impossible at 40 °C. At high temperature, i.e., 100 °C, H_2O_2 was unstable and part of it decomposed into water and molecular oxygen which decreased the concentration of active oxygen species on the catalyst surface; this is absolutely unfavorable to the DBT oxidation. It is noted that acetonitrile was evaporated at around 82 °C and thus extracting agent was under reflection condition, which disfavors the extraction of the formed sulfone. At 60–80 °C, the highest DBT conversion was obtained. This was probably due to the appropriate interaction of the oxidant with the catalyst that accelerated the formation of peroxometallic species and enhanced the DBT oxidation efficiency. According to our results, the best DBT removal efficiency can be achieved at the reaction temperature between 60 °C and 80 °C.

2.6.3. Effect of Reaction Time and Vanadia Loading

It is noteworthy that the DBT oxidation reaction under the present experimental condition was very rapid. In the first 10 min of reaction, more than 70.0% and 82.4% of DBT were oxidized on the V_2O_5 /SBA-15 and V_2O_5 /Zr-SBA-15 catalysts, respectively (Figure 9). After 30–40 min of the reaction, greater than 95.0% of DBT were removed and the DBT conversion remained almost constant in the following treatment. This is probably related to the rapid generation of surface reactive oxygen species. When H_2O_2 and catalysts were added into the reaction system, peroxyoxide and superoxide species were rapidly generated on the active sites of the catalyst in the initial stage of the reaction.

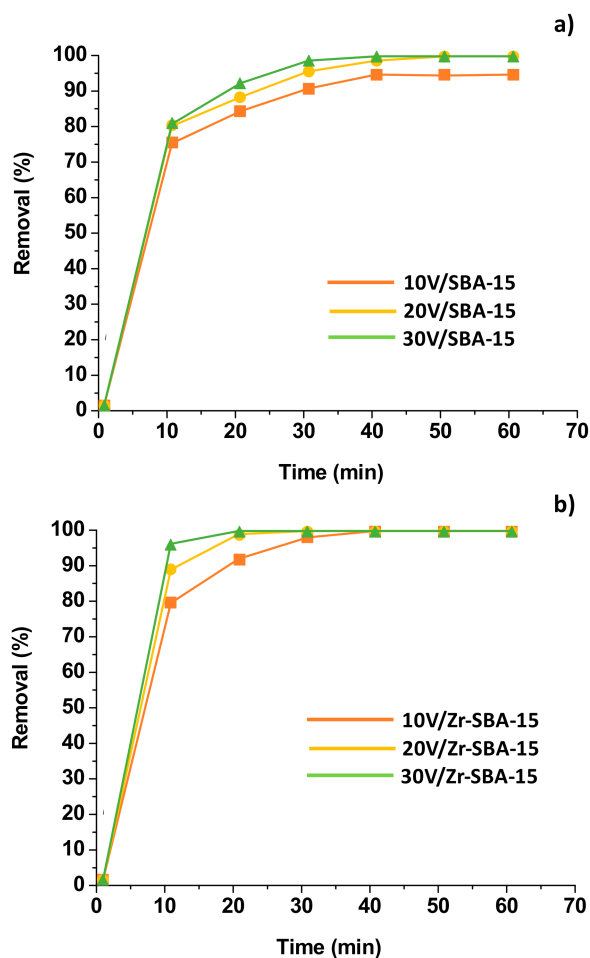


Figure 9. Effect of reaction time and vanadia loading. Reaction conditions: catalyst loading: 1 g/L oil; reaction temperature: 60 °C; H₂O₂/DBT molar ratio: 10; reaction time: 60 min; oil/acetonitrile volume ratio: 1:1. (a) V₂O₅/SBA-15; (b) V₂O₅/Zr-SBA-15.

The DBT conversion increased by increasing the vanadia loading, showing an increasing order as:

$$10\% \text{ V}_2\text{O}_5/\text{SBA-15} < 20\% \text{ V}_2\text{O}_5/\text{SBA-15} < 30\% \text{ V}_2\text{O}_5/\text{SBA-15} \quad (1)$$

$$10\% \text{ V}_2\text{O}_5/\text{Zr-SBA-15} < 20\% \text{ V}_2\text{O}_5/\text{Zr-SBA-15} < 30\% \text{ V}_2\text{O}_5/\text{Zr-SBA-15} \quad (2)$$

This is because that the catalysts with higher V₂O₅ content present a greater number of active sites and higher surface density of Lewis acid sites, and thus they are more active for DBT oxidation. Considering the cost of catalyst, we did not prepare catalysts with vanadia content greater than 30 wt%. In comparison with MoO₃/SBA-15 [33], CoMo/SBA-15 [34], and WO₃/SBA-15 [37], and FeOx/Zr-SBA-15 [56], the V₂O₅/SBA-15 and V₂O₅/Zr-SBA-15 are the most active catalysts for DBT oxidation under the similar reaction condition.

2.6.4. Catalyst Reusability Tests

Figure 10 shows the catalytic activity of 30% V₂O₅/Zr-SBA-15 catalyst evaluated by repeating 8 runs under the optimal reaction condition (60 °C, catalyst concentration 1 g/L oil, R = 10, and reaction time 60 min). At the end of each experiment, the catalyst was filtered and dried, and then used for the next test. We found that the 30% V₂O₅/Zr-SBA-15 catalyst showed almost the same DBT conversion for the first two recycles, higher than 98.1%. For the reaction that runs from the third to sixth, the catalytic activity slightly diminished by evidenced the DBT conversion decrease by 4–5%.

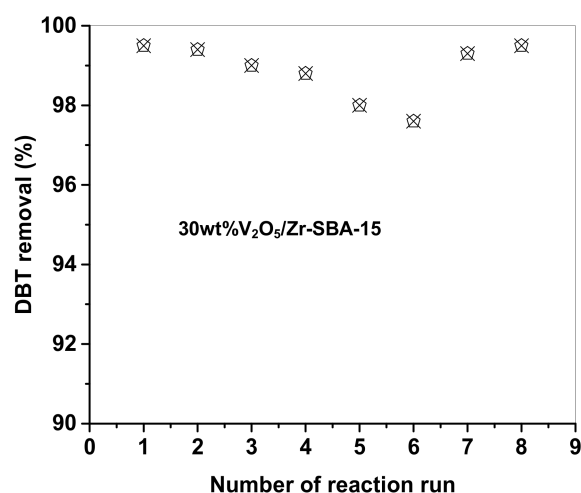


Figure 10. Reusability test of the 30 wt% $V_2O_5/Zr-SBA-15$ catalyst. Reaction condition: catalyst loading: 1 g/L oil; H_2O_2/DBT molar ratio: 10; reaction temperature: 60 °C; reaction time: 60 min; oil/acetonitrile volume ratio: 1:1. The test No. 7 was carried out by adding a small amount fresh catalyst in order to remain the catalyst mass the same amount as used for the first run. The test No. 8 was performed using the calcined catalyst obtained after reaction run No. 6 by adding a small amount of fresh catalyst in order to keep the catalyst mass the same as was used for the first reaction run.

For further searching for the reasons of the catalytic activity diminishing, we particularly designed two additional tests for the 30% $V_2O_5/Zr-SBA-15$ catalyst after 6 times of recycling: (i) adding a little bit of fresh catalyst in order to remain the catalyst mass the same as used in the first test (terms reaction run No. 7); and (ii) the reused catalyst was washed with methanol and calcined in air at 400 °C and then a little bit of fresh catalyst was added in order to remain the catalyst mass the same as used in the first test (terms reaction run No. 8). Results showed in run No. 7 that the 30% $V_2O_5/Zr-SBA-15$ catalyst recovered 98% of the initial activity without calcination. After calcination, the 30% $V_2O_5/Zr-SBA-15$ catalyst achieved almost the same activity as the fresh one. These results confirmed that the slight diminishing of the catalyst activity resulted from the catalyst mass loss due to the filtration operation and the washing procedure as well as by partial coverage of the active sites by the adsorbed DBT. Moreover, if V leaching took place, some active sites permanently disappear. However, in our experiment No. 8, the catalytic activity reached the same level obtained in reaction run No. 1. This result indicates that V leaching may not occur during the 6 successive reaction cycles.

3. Discussion

3.1. Roles of Ultrasound and Surfactant in the Synthesis

In the absence of the ultrasound, the hydrothermal synthesis of SBA-15 and Zr-SBA-15 took approximately 48–72 h. In the present work, when the ultrasound was applied, the synthesis time shortened to 24 h. This is because ultrasound could nebulize solutions into fine mixtures and accelerate chemical reactions. Furthermore, the ultrasound favored dispersing nanoparticles and colloids in the reaction mixture and thus benefits the reduction of crystal size of the solid [60–62]. Ultrasound also significantly reduces the mass transfer limitation between phases in heterogeneous systems by excellent dispersion. The acoustic waves with frequencies higher than 20 kHz (40 kHz in the presence work) interacted with reaction species, disrupted the weak noncovalent interactions, or disintegrated the aggregated particles. All these factors resulted in a smaller particle size.

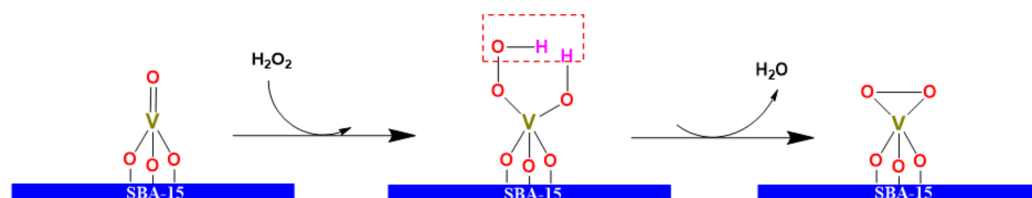
In the impregnation of the vanadium precursor on the SBA-15 and Zr-SBA-15 supports, a proper amount (depending of the volume of the suspended mixture, 1 g was added in the present experiment) of Surfapcol 9030-S was used to lower the surface tension of

the mixture of the vanadium precursor. Surfapcol 9030-S addition prevented vanadia agglomeration and avoid large particles formation on the support surface.

3.2. Influence of Surface Peroxometallic Species

Raman characterization showed that both β - V_2O_5 and α - V_2O_5 phases were formed on the surface of the catalysts. The structure of β - V_2O_5 has layers (on the y-z plane) of edge and corner shared VO_6 octahedra which is twice as thick as the layer of the α - V_2O_5 phase along a-axis. The polyhedral layers in β - V_2O_5 form a key-lock geometry where polyhedral units in one layer are just above the voids in the next layer [58,59]. This gives rise to formation of more O–O, V–O and V=O between the polyhedral layers in β - V_2O_5 as compared to that in α - V_2O_5 . In the ODS reaction, the double V=O bonds are stretching out and therefore they were easily attacked by oxidant H_2O_2 to form peroxometallic V–O–O–H species [63].

The DBT conversion increased on increasing of vanadia content in the catalysts (see Figure 9). Two possible reasons may be responsible for the enhancement of DBT conversion along with the vanadia content: (i) V^{5+} ions are the centers of Lewis acidity because they have unoccupied 3d orbitals in the electron configuration, which may also serve as electron acceptors for DBT adsorption. In fact, XPS characterization confirmed that some V^{4+} ions are formed in the catalysts [38,40]. V^{4+} ions formation indicated that oxygen defects are created as neighbors of V^{5+} ions for charge balance. Therefore, oxygen defects are one of the origins of Lewis acid sites; (ii) V^{5+} ions are the sites for the formation of peroxometallic complexes resulting from the interaction between hydrogen peroxide and unoccupied 3d electron orbitals of V^{5+} . Compared with pure H_2O_2 , the peroxometallic complexes V^{5+} –O–O–H were more stable and more effective for the ODS reaction; because the V–O–O–H bond is unsymmetrical, and the electron density in the O–O bond of V–O–O–H species is unbalanced, thus the dissymmetry O–O bond has strong polarization [64–66]. V–O–O–H species may further transfer to the peroxovanadium complexes V–O–O–V by releasing one water molecule (Scheme 1). The electrons were withdrawn from the peroxy moiety and increased the electrophilic character of the peroxidic oxygens, favoring the oxygen atom transfer to the S atom in the DBT molecule.



Scheme 1. A mechanism of preoxovanadium complex formation.

3.3. Correlation of Lewis Acidity with DBT Conversion

The in situ pyridine adsorption of FTIR measurements confirmed that V_2O_5 /SBA-15 and V_2O_5 /Zr-SBA-15 catalysts contained many Lewis acid sites. The DBT molecule has one S atom which has two isolated electron pairs; and therefore, DBT possesses a Lewis base character as electron donor. Lewis acid sites in the catalyst surface can serve as electron acceptors for DBT adsorption. In the initial stage of the ODS procedure, DBT molecule preferentially adsorbed on Lewis acid sites via denoting its electron pairs in sulfur atom to Lewis acid sites.

DBT conversion against the amount of Lewis acidity is plotted in Figure 11. It demonstrates that DBT conversion achieved with the V_2O_5 /SBA-15 or V_2O_5 /Zr-SBA-15 catalysts at 40 °C (Figure 11a) and at 60 °C (Figure 11b) were almost proportional to the amount of Lewis acidity. Therefore, increasing Lewis acid sites by loading transition metal oxides or creating more crystalline structural defects in the heterogeneous catalysts is an effective route to enhance DBT oxidation activity.

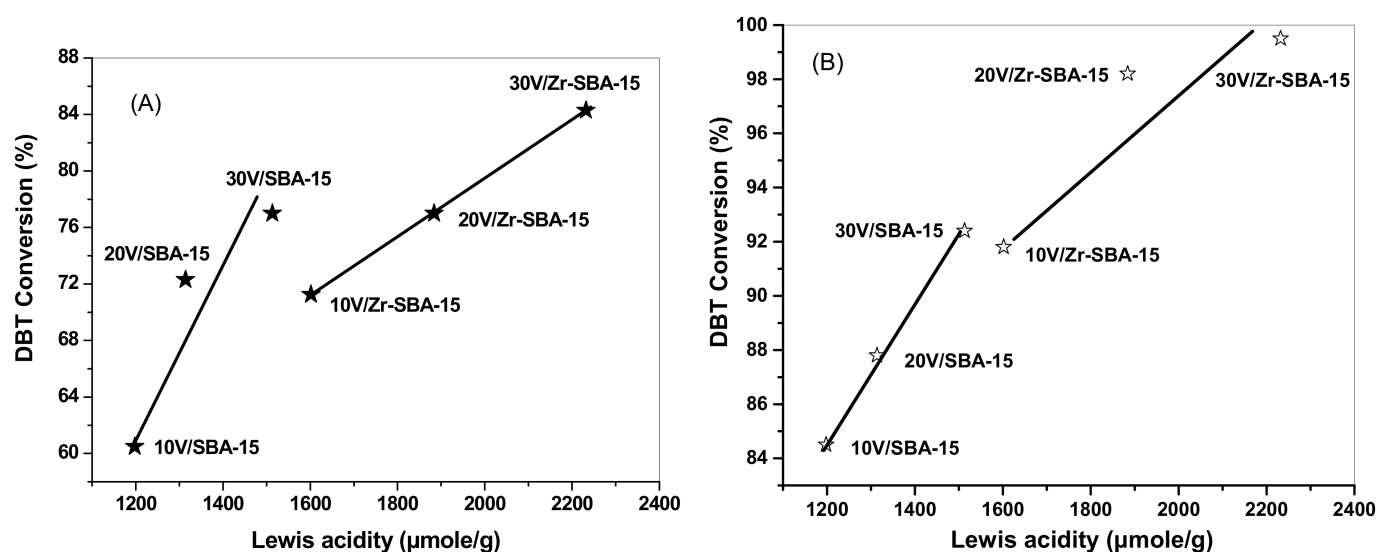


Figure 11. DBT conversion as a function of Lewis acidity of the catalysts. (A) DBT conversion data were obtained at 40 °C after 60 min of reaction and the Lewis acidity data were obtained at 100 °C. (B) DBT conversion data were obtained at 60 °C after 20 min of reaction and the Lewis acidity data were obtained at 100 °C.

It is noted that $V_2O_5/SBA-15$ and $V_2O_5/Zr-SBA-15$ catalysts also present some B acid sites; however, the value of B/L ratio is very small, ranging between 0.006 and 0.04. Although we cannot rule out the possibility of the B acidity participation in the DBT oxidation, its effect is less important in the present work.

3.4. Effects of Zirconium Modification

The replacement of Si^{4+} by Zr^{4+} in the framework of SBA-15 was confirmed by the FTIR characterization (See the Supplementary Materials Figure S1), where one band at 965 cm^{-1} in the $V_2O_5/SBA-15$ catalysts was observed; it was assigned to the formation of the Si–O–H bond in the SBA-15 structure. This band shifts its position from 965 cm^{-1} in the FTIR spectra of $V_2O_5/SBA-15$ to $975\text{--}980\text{ cm}^{-1}$ for the $V_2O_5/Zr-SBA-15$ catalysts, indicating that H^+ in the Si–O–H species in SBA-15 was replaced by Zr^{4+} to form the Si–O–Zr bond [67,68].

Because Zr^{4+} has the same positive charge as Si^{4+} but with larger size (Zr^{4+} radius is 84 pm and Si^{4+} radius is 44 pm), when Zr^{4+} ions were inserted into the SBA-15 framework to replace some Si^{4+} or occupy the lattice vacancies, the Si–O–Zr bond was formed. This replacement could result in distortion or deformation of the tetrahedral environment of Zr–O–Si in the Zr-SBA-15 due to the charge unbalance and the lattice cell volume modification, generating new acid sites.

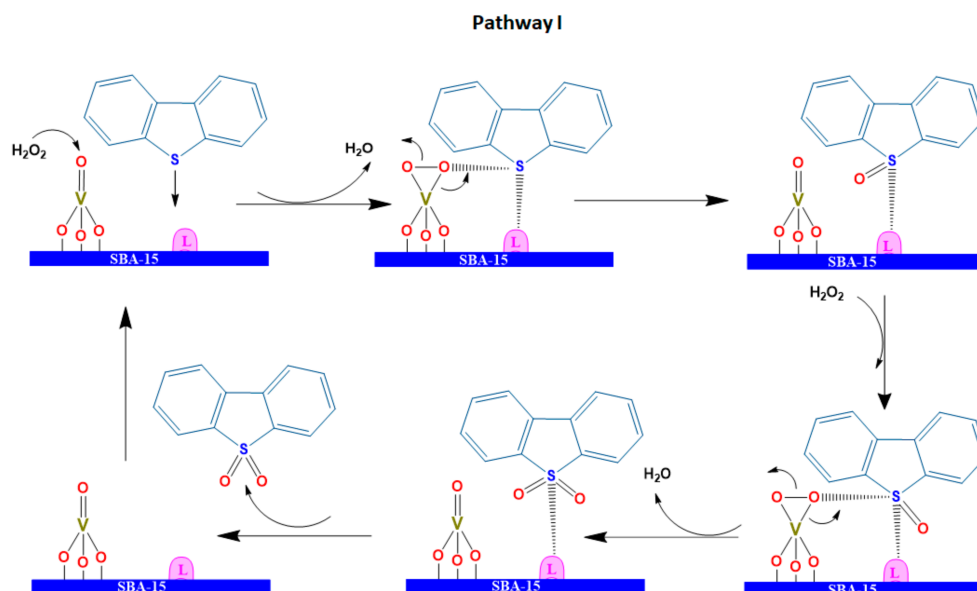
In comparison with SBA-15, Zr-doped SBA-15 has higher textural stability and enhanced surface acidity. As seen in Table 2, all the $V_2O_5/Zr-SBA-15$ catalysts showed a larger amount of Lewis acid sites than that of $V_2O_5/SBA-15$ catalysts. These results clearly evidenced that Zr^{4+} ions promoted the formation of additional acid sites.

It is observed that a small amount of t- ZrO_2 was segregated from the 30 wt% $V_2O_5/Zr-SBA-15$ catalyst, which probably results from the replacement of Zr^{4+} by V^{5+} because the segregation was not observed in the Zr-SBA-15 sample. Zr^{4+} ionic radius is 84 pm which is almost double of Si^{4+} ionic radius (44 pm). However, the V^{5+} radius is 59 pm which is similar to that of Si^{4+} . The replacement of Zr^{4+} ion by V^{5+} may decrease the tension force in SBA-15 framework and the degree of structure deformation.

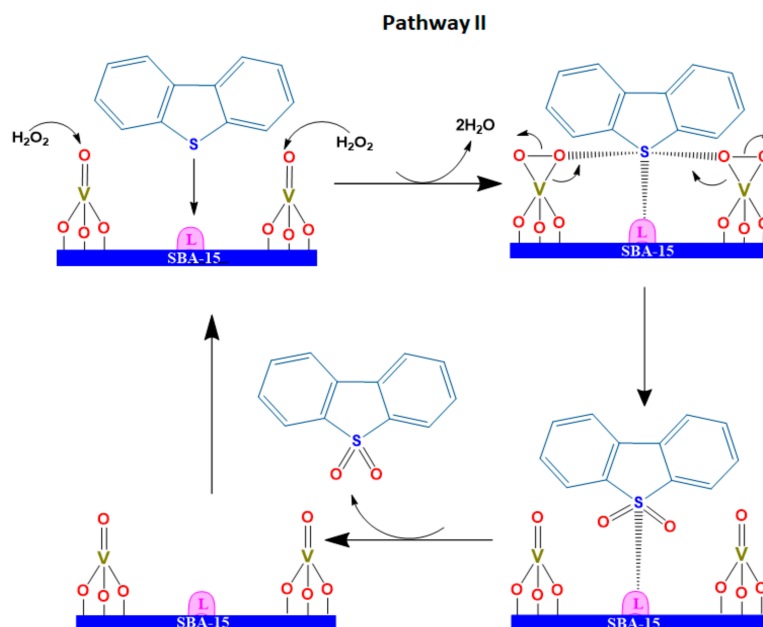
3.5. ODS Mechanism

It is reported that W=O and Mo=O can be transferred into W–O–O and Mo–O–O surface preoxometallic oxygen species with H_2O_2 oxidation; these served as active oxygen species for sulfur oxidation in the ODS reactions [69,70]. On the basis of the above results

and discussion, we proposed reaction mechanisms of DBT oxidation and removal in Schemes 1–3. For the catalyst with low vanadia loading, for instance, 10 wt% V_2O_5 , where the vanadia crystallite size is small and some isolated small V_2O_5 crystals or clusters may be highly dispersed on the surface of the catalysts. In the ODS reaction mixture, H_2O_2 was first coordinated with $V=O$ to form $V^{5+}-O-O-H$ and finally to the peroxovanadium complex (VO_2 species) by releasing one H_2O molecule (Scheme 1).



Scheme 2. DBT oxidation via Pathway I on the catalyst with low vanadia loading.



Scheme 3. DBT oxidation via Pathway II on the catalyst with moderate vanadia loading.

For the ODS reaction, the DBT molecule is preferentially adsorbed on L acid sites via denoting its electron pairs in the sulfur atom to L acid sites. In an ideal case, peroxovanadium species connected on the surface of the catalysts where DBT was adsorbed in Lewis sites as neighbors, so the oxygen atom in the peroxovanadium complex species (VO_2) transferring to DBT became relatively easier, forming a dibenzosulfoxide intermediate. As the reaction proceeds further, peroxometallic species react with the dibenzosulfoxide

again to transfer another oxygen atom, finally producing a sulfone molecule (Scheme 2, Pathway I).

The vanadia concentration and dispersion strongly affects the ODS activity [40]. For the catalyst with moderate vanadia loading, herein 20–30 wt% V_2O_5 , where distance between vanadia crystals may be short due to the higher concentration of surface vanadia nanoparticles. Therefore, two neighboring vanadia nanocrystals may simultaneously participate in the oxidation of the same DBT molecule. This may benefit the DBT oxidation with higher efficiency and more rapid via the Pathway II as described in Scheme 3. In these catalysts, DBT oxidation may proceed via the Pathway I and the Pathway II simultaneously, promoting the rapid and complete ODS reaction. This explains the high catalytic activity of the 30 wt% V_2O_5 /SBA-15 and 30 wt% V_2O_5 /Zr-SBA-15 catalysts. A too-high vanadia loading may lead to poor dispersion and a larger crystallite size that are unfavorable to the enhancement of DBT adsorption and oxidation [38,40]. On the basis of previous experimental experience, we did not investigate the catalyst activity with vanadia content greater than 30 wt%.

It is noted that an adsorption competition between DBT and hydrogen peroxide oxidant may occur on the same site, herein V^{5+} ions, because both DBT and hydrogen peroxide possess electron-rich or Lewis base character. This adsorption competition accelerated the oxygen transfer from the oxidant to DBT and benefited the enhancement of ODS efficiency.

In our designed ODS reaction system, the ODS operation combines the oxidation of DBT and the extraction of resultant products by acetonitrile. DBT oxidation and sulfone separation can be simultaneously performed in a one-pot operation unit, making it practical and attractive for clean fuels production.

4. Materials and Methods

4.1. Synthesis of SBA-15, Zr-SBA-15, V_2O_5 /SBA-15, and V_2O_5 /Zr-SBA-15

SBA-15 and Zr-SBA-15 supports were prepared by an ultrasound-assisted hydrothermal method. Tetraethylorthosilicate (TEOS) was used as Si precursor, zirconium butoxide (IV) (80 wt% solution in 1-butanol, Sigma, St. Louis, MO, USA) was used as Zr starting chemical, and triblock copolymer P123 was used as structural linker. For the synthesis of Zr-SBA-15, the Si/Zr molar ratio was set at 10, which corresponds to a Zr content 12.60 wt% in Zr-SBA-15 solid. In the synthesis procedure, the ultrasound-assisted hydrothermal method with an ultrasonic generator (Brasonic 5510R-DTH at 42 kHz frequency, Marshall Scientific, Boston, MA, USA) was applied. The obtained solids were calcined under flow air at 550 °C for 6 h. The experimental details for SBA-15 and Zr-SBA-15 synthesis can be seen in references [34,54].

The vanadia dispersed on SBA-15 or Zr-SBA-15 catalysts were prepared by the wet impregnation method. First, 5 g of SBA-15 or Zr-SBA-15 solid were impregnated with 150 mL aqueous solution containing a calculated amount of ammonium metavanadate (NH_4VO_3 , 99%, Sigma-Aldrich, Toluca, Mexico) in order to obtain the vanadia load of 10, 20, and 30 wt% in the final catalysts. 1 g Surfapcol 9030-S (70%, Mexico City, Mexico) was added in order to lower the surface tension of the solution. The suspended mixture was heated at 95 °C in a rotary evaporator. After water was evaporated, the solid powders were dried at 110 °C for 12 h and then calcined at 500 °C for 6 h in air flow. The obtained solids termed as nV/SBA-15 and nV/Zr-SBA-15 catalysts (sometimes, they are also written as nV_2O_5 /SBA-15 or nV_2O_5 /Zr-SBA-15) where n indicates the V_2O_5 weight percentage.

4.2. Crystalline Characterization

XRD patterns of V/SBA-15 and V/Zr-SBA-15 catalysts were obtained with an X-ray diffractometer (Siemens D500, Munich, Germany) using $Cu K\alpha$ radiation ($\lambda = 1.5405 \text{ \AA}$). Textural properties of support and catalysts were measured by the N_2 adsorption-desorption isotherms method, which was performed on a Nova 4000 Series instrument (Quantachrome Instruments, Boynton Beach, FL, USA). Scanning electron microscopy (SEM) (Quanta 3D FEG Microscope with Brand FEI, Tokyo, Japan) was used to observe the morphological

features of the support and the catalysts. For close observation of crystallite size and the dispersion of vanadia on the support, high resolution transmission electron microscopy (TEM) was applied (JEM-ARM200CF model, JEOL, Tokyo, Japan). The surface species of the catalysts were investigated by the Raman spectroscopic technique (LabRAM HR800 model, HORIBA, France) with a 532 nm line laser excitation and a 3D filter. The Raman spectra were recorded in the wavenumber range between 100 cm^{-1} and 1200 cm^{-1} . The surface acidity of the support and catalysts was measured with in situ Fourier transform infrared (FTIR) spectroscopy of pyridine adsorption technique on a FTIR spectrometer (Perkin-Elmer Model 170-SX, Waltham, MA, USA). The IR spectra were recorded at different temperatures ranging from 25 to $400\text{ }^{\circ}\text{C}$. The IR absorption band at approximately 1450 cm^{-1} was used to monitor the Lewis acidity; and the IR band at around 1540 cm^{-1} was used to calculate the Brønsted acidity. The extinction coefficients $E_B = 1.0086\text{ mmol/cm}^2$ for Brønsted acid sites and $E_L = 0.9374\text{ mmol/cm}^2$ for Lewis acid sites were used for the acidity calculation.

4.3. Catalytic Activity Evaluation

The ODS reaction of a model diesel consisting of n-hexadecane and 300 ppm of DBT was carried out in a glass reactor. In a typical test, the glass reactor contained 50 mL of the model fuel and 50 mL of acetonitrile (Fermont, 99.8%, Monterrey, Canada). In some experiments, in order to reduce the operation cost, 30 mL model fuel and 30 mL of solvent were used. Hydrogen peroxide (Sigma-Aldrich, 30 vol% H_2O_2 in water, St. Louis, MO, USA) as oxidant was added into the reaction system at different $\text{H}_2\text{O}_2/\text{DBT}$ molar ratios varying from 2 to 15; the catalyst was added at a concentration of 1 g/L of oil. Thus, the ODS operation system was a three-phase mixture of a nonpolar phase (liquid oil), a polar phase (liquid acetonitrile/ H_2O_2), and a solid (catalyst). The reaction temperature varied between 40 and $100\text{ }^{\circ}\text{C}$ under stirring with an electromagnetic rod. The reaction time was controlled for 60 min. Each time, 10 μL reaction mixture were taken at 10 min of reaction and it was diluted with 5 mL ethyl alcohol. Then they were filtered with a 0.45 μL organic filter membrane for the separation of the catalyst particles. Finally, the UV-vis spectra of the diluted solution sample were recorded with an ultraviolet-visible (UV-vis) spectrometer. The catalytic activity of the catalysts was demonstrated as DBT conversion.

5. Conclusions

Several important conclusions have been drawn from this work:

1. The ultrasound-assisted hydrothermal method and surfactant addition in the synthesis of both, the SBA-15 and Zr-SBA-15 supports and the vanadia loaded catalysts, could shorten the synthesis time from 72 h to 24 h and prevented the formation of vanadia with large agglomerates on the surface of the support.
2. Zr addition in the synthesis procedure of SBA-15 formed the Zr-O-Si bond and significantly improved the stability of textural properties and created more Lewis acid sites on the catalysts.
3. All the $\text{V}_2\text{O}_5/\text{SBA-15}$ and $\text{V}_2\text{O}_5/\text{Zr-SBA-15}$ catalysts presented a large amount of Lewis acid sites. The DBT oxidation was found to be a Lewis acidity sensitive reaction where DBT molecule preferentially adsorbed on the Lewis sites of the catalyst via denoting its isolated electron pairs to Lewis acid centers. Creating more Lewis acidity in a catalyst by structural or/and surface modifications is an effective route to improve the efficiency of DBT oxidation.
4. Under the optimal reaction condition (Reaction temperature: $60\text{ }^{\circ}\text{C}$, reaction time 40 min, catalyst concentration: 1 g/L oil; $\text{H}_2\text{O}_2/\text{DBT}$ mole ratio = 10), the best catalyst 30 wt% $\text{V}_2\text{O}_5/\text{Zr-SBA-15}$ could remove more than 99% DBT from the model diesel.
5. A mechanism involving DBT adsorption on Lewis acid sites, formation of peroxometallic complexes such as V-O-O-H, oxygen atom transfer between peroxovanadium complexes and adsorbed DBT, generation of sulfone in the interface and separation from the oil phase by polar extraction, was proposed for the ODS reaction. In the

case of low vanada loading ($V_2O_5 \leq 10$ wt%), ODS may occur through Pathway I; in the catalysts with moderate vanadia content ($V_2O_5 = 20\text{--}30$ wt%), ODS may proceed via Pathway II and Pathway I.

6. The designed reaction system consisting of a green oxidant (H_2O_2), a mesoporous catalyst carrying on predominant Lewis acidity ($V_2O_5/Zr\text{-SBA-15}$), and a polar solvent (acetonitrile) was designed for simultaneous oxidation and separation of DBT in one-pot operation unit, which is quite attractive and practical for the production of ultralow sulfur fuel.

Supplementary Materials: The following are available online at <https://www.mdpi.com/2073-4344/11/4/408/s1>, Figure S1 FTIR spectra of the $V_2O_5/SBA-15$ and $V_2O_5/Zr\text{-SBA-15}$.

Author Contributions: Conceptualization, J.A.W.; Methodology, J.N., U.A. and J.M.R.; Investigation, J.M.R., U.A. and J.G.; Writing—J.M.R. and J.A.W.; Writing—Review & Editing, L.C. and L.E.N.; Supervision, J.A.W. and S.O.F.; Funding Acquisition, J.A.W., L.C. and L.E.N. All authors have read and agreed to the published version of the manuscript.

Funding: The financial support obtained from projects of Instituto Politécnico Nacional Grant No. SIP-20196124, SIP-20196194, and SIP-20201639 is appreciated.

Acknowledgments: The authors thank the Centro de Nanociencias y Micro y NanoTecnologías del Instituto Politécnico Nacional for technical support. J.M. Ramos thanks the doctoral scholarship offered by CONACyT-Mexico.

Conflicts of Interest: The authors claim that there is no interest conflict.

References

1. Rezvani, M.A.; Shaterian, M.; Aghbolagh, Z.S.; Babaei, R.; Kabe, T.; Ishihara, A.; Qian, W. *Hydrodesulfurization and Hydrodenitrogenation: Chemistry and Engineering*, 7th ed.; Wiley-VC: Weinheim, NY, USA, 1999; pp. 112–232.
2. Hossain, M.N.; Park, H.C.; Choi, H.S. A comprehensive review on catalytic oxidative desulfurization of liquid fuel oil. *Catalysts* **2019**, *9*, 229. [CrossRef]
3. Song, C. An overview of new approaches to deep desulfurization for ultra-clean gasoline, diesel fuel and jet fuel. *Catal. Today* **2003**, *86*, 211–263. [CrossRef]
4. Stanislaus, A.; Marafi, A.; Rana, M.S. Recent advances in the science and technology of ultralow sulfur diesel (ULSD) Production. *Catal. Today* **2010**, *153*, 1–68. [CrossRef]
5. Gawande, P.R.; Kaware, J. Desulphurization techniques for liquid fuel: A review. *Int. J. Eng. Technol. Manag. Appl. Sci.* **2014**, *2*, 121–127.
6. Cho, K.-S.; Lee, Y.-K. Effects of nitrogen compounds, aromatics, and aprotic solvents on the oxidative desulfurization (ODS) of light cycle oil over Ti-SBA-15 catalyst. *Appl. Catal. B Environ.* **2014**, *147*, 35–42. [CrossRef]
7. Babich, J.I.; Moulijn, J.A. Science and technology of novel processes for deep desulfurization of oil refinery streams: A review. *Fuel* **2003**, *82*, 607–631. [CrossRef]
8. Anderson, K.; Atkins, M.P.; Borges, P.; Chan, Z.P.; Rafeen, M.S.; Sebran, N.H.; Van Der Pool, E.; Vleeming, J.H. Economic analysis of ultrasound-assisted oxidative desulfurization. *Energy Sources Part B Econ. Plan. Policy* **2017**, *49*, 1–7. [CrossRef]
9. Maghsoudi, S.; Vossoughi, M.; Kheirloomoom, A.; Tanaka, E.; Katoh, S. Biodesulfurization of hydrocarbons and diesel fuels by *Rhodococcus* sp. strain P32C1. *Biochem. Eng. J.* **2001**, *8*, 151–156. [CrossRef]
10. Monticello, D.J. Biodesulfurization and the upgrading of petroleum distillates. *Curr. Opin. Biotechnol.* **2000**, *11*, 540–546. [CrossRef]
11. Soleimani, M.; Bassi, A.; Margaritis, A. Biodesulfurization of refractory organic sulfur compounds in fossil fuels. *Biotechnol. Adv.* **2007**, *25*, 570–596. [CrossRef]
12. Abin-Fuentes, A.; Leung, J.C.; Mohamed, M.E.-S.; Wang, D.I.; Prather, K.L. Rate-limiting step analysis of the microbial desulfurization of dibenzothiophene in a model oil system. *Biotechnol. Bioeng.* **2013**, *111*, 876–884. [CrossRef] [PubMed]
13. Abin-Fuentes, A.; Mohamed, M.E.-S.; Wang, D.I.C.; Prather, K.L.J. Exploring the mechanism of biocatalyst inhibition in microbial desulfurization. *Appl. Environ. Microbiol.* **2013**, *79*, 7807–7817. [CrossRef] [PubMed]
14. Yazu, K.; Yamamoto, Y.; Furuya, T.; Miki, K.; Ukegawa, K. Oxidation of dibenzothiophenes in an organic biphasic system and its application to oxidative desulfurization of light oil. *Energy Fuels* **2001**, *15*, 1535–1536. [CrossRef]
15. Ishihara, A.; Wang, D.; Dumeignil, F.; Amano, H.; Qian, E.W.; Kabe, T. Oxidative desulfurization and denitrogenation of a light gas oil using an oxidation/adsorption continuous flow process. *Appl. Catal. A Gen.* **2005**, *279*, 279–287. [CrossRef]
16. Hasan, Z.; Jeon, J.; Jhung, S.H. Oxidative desulfurization of benzothiophene and thiophene with WO_x/ZrO_2 catalysts: Effect of calcination temperature of catalysts. *J. Hazard. Mater.* **2012**, *205–206*, 216–221. [CrossRef] [PubMed]

17. Sarda, K.; Bhandari, A.; Pant, K.; Jain, S. Deep desulfurization of diesel fuel by selective adsorption over Ni/Al₂O₃ and Ni/ZSM-5 extrudates. *Fuel* **2012**, *93*, 86–91. [[CrossRef](#)]
18. Mužić, M.; Sertić-Bionda, K.; Gomzi, Z.; Podolski, Š.; Telen, S. Study of diesel fuel desulfurization by adsorption. *Chem. Eng. Res. Des.* **2010**, *88*, 487–495. [[CrossRef](#)]
19. Hernández-Maldonado, A.J.; Yang, R.T. New sorbents for desulfurization of diesel fuels via π -complexation. *AIChE J.* **2004**, *50*, 791–801. [[CrossRef](#)]
20. Kim, J.H.; Ma, X.; Zhou, A.; Song, C. Ultra-deep desulfurization and denitrogenation of diesel fuel by selective adsorption over three different adsorbents: A study on adsorptive selectivity and mechanism. *Catal. Today* **2006**, *111*, 74–83. [[CrossRef](#)]
21. Yu, G.X.; Jin, M.; Sun, J.; Zhou, X.L.; Chen, L.F.; Wang, J.A. Oxidative modifications of rice hull-based carbons for dibenzothiophene adsorptive removal. *Catal. Today* **2013**, *212*, 31–37. [[CrossRef](#)]
22. Joskić, R.; Margeta, D.; Sertić, K. Oxidative desulfurization of model diesel fuel with hydrogen peroxide. *Goriva i Maziva.* **2014**, *53*, 11–18.
23. Mamaghani, A.H.; Fatemi, S.; Asgari, M. Investigation of influential parameters in deep oxidative desulfurization of dibenzothiophene with hydrogen peroxide and formic acid. *Int. J. Chem. Eng.* **2013**, *2013*, 951045. [[CrossRef](#)]
24. Yu, G.; Lu, S.; Chen, H.; Zhu, Z. Diesel fuel desulfurization with hydrogen peroxide promoted by formic acid and catalyzed by activated carbon. *Carbon* **2005**, *43*, 2285–2294. [[CrossRef](#)]
25. Wang, D.; Qian, E.W.; Amano, H.; Okata, K.; Ishihara, A.; Kabe, T. Oxidative desulfurization of fuel oil, part I. Oxidation of dibenzothiophenes using tert-butyl hydroperoxide. *Appl. Catal. A Gen.* **2003**, *253*, 91–99. [[CrossRef](#)]
26. Murata, S.; Murata, K.; Kidena, A.K.; Nomura, M. A novel oxidative desulfurization system for diesel fuels with molecular oxygen in the presence of cobalt catalysts and aldehydes. *Energy Fuels* **2004**, *18*, 116–121. [[CrossRef](#)]
27. Bhutto, A.W.; Abro, R.; Gao, S.; Abbas, T.; Chen, X.; Yu, G. Oxidative desulfurization of fuel oils using ionic liquids: A review. *J. Taiwan Inst. Chem. Eng.* **2016**, *62*, 84–97. [[CrossRef](#)]
28. Wang, J.; Zhang, L.; Sun, Y.; Jiang, B.; Chen, Y.; Gao, X.; Yang, H. Deep catalytic oxidative desulfurization of fuels by novel Lewis acidic ionic liquids. *Fuel Process. Technol.* **2018**, *177*, 81–88. [[CrossRef](#)]
29. Dharaskar, S.A.; Wasewar, K.L.; Varma, M.N.; Shende, D.Z.; Yoo, C. Synthesis, characterization and application of 1-butyl-3-methylimidazolium tetrafluoroborate for extractive desulfurization of liquid fuel. *Arab. J. Chem.* **2016**, *9*, 578–587. [[CrossRef](#)]
30. Li, X.; Zhang, J.; Zhou, F.; Wang, Y.; Yuan, X.; Wang, H. Oxidative desulfurization of dibenzothiophene and diesel by hydrogen peroxide: Catalysis of H₃PMo₁₂O₄₀ immobilized on the ionic liquid modified SiO₂. *Mol. Catal.* **2018**, *452*, 93–99. [[CrossRef](#)]
31. Zhang, L.; Wang, J.; Sun, Y.; Jiang, B.; Yang, H. Deep oxidative desulfurization of fuels by superbases-derived Lewis acidic ionic liquids. *Chem. Eng. J.* **2017**, *328*, 445–453. [[CrossRef](#)]
32. Al-Shahrani, F.; Xiao, T.; Llewellyn, S.A.; Barri, S.; Jiang, Z.; Shi, H.; Martinie, G.; Green, M.L. Desulfurization of diesel via the H₂O₂ oxidation of aromatic sulfides to sulfones using a tungstate catalyst. *Appl. Catal. B Environ.* **2007**, *73*, 311–316. [[CrossRef](#)]
33. González, J.; Wang, J.A.; Chen, L.; Manríquez, M.; Salmones, J.; Limas, R.; Arellano, U. Quantitative determination of oxygen defects, surface lewis acidity, and catalytic properties of mesoporous MoO₃/SBA-15 catalysts. *J. Solid State Chem.* **2018**, *263*, 100–114. [[CrossRef](#)]
34. Ramos, J.M.; Wang, J.A.; Chen, L.F.; Arellano, U.; Ramírez, S.P.; Sotelo, R.; Schachat, P. Synthesis and catalytic evaluation of CoMo/SBA-15 catalysts for oxidative removal of dibenzothiophene from a model diesel. *Catal. Commun.* **2015**, *72*, 57–62. [[CrossRef](#)]
35. Maciua, A.-L.; Ciocan, C.-E.; Dumitriu, E.; Fajula, F.; Hulea, V. V. Mo- and W-containing layered double hydroxides as effective catalysts for mild oxidation of thioethers and thiophenes with H₂O₂. *Catal. Today* **2008**, *138*, 33–37. [[CrossRef](#)]
36. Xiao, X.; Zhong, H.; Zheng, C.; Lu, M.; Zuo, X.; Nan, J. Deep oxidative desulfurization of dibenzothiophene using a flower-like WO₃·H₂O catalyst in an organic biphasic system. *Chem. Eng. J.* **2016**, *304*, 908–916. [[CrossRef](#)]
37. Gonzalez, J.; Wang, J.A.; Chen, L.; Manriquez, M.E.; Dominguez, J.M. Structural defects, lewis acidity, and catalysis properties of mesostructured WO₃/SBA-15 nanocatalysts. *J. Phys. Chem. C* **2017**, *121*, 23988–23999. [[CrossRef](#)]
38. González, J.; Chen, L.; Wang, J.A.; Manríquez, M.E.; Limas, R.; Schachat, P.; Navarrete, J.; Contreras, J. Surface chemistry and catalytic properties of VO_x/Ti-MCM-41 catalysts for dibenzothiophene oxidation in a biphasic system. *Appl. Surf. Sci.* **2016**, *379*, 367–376. [[CrossRef](#)]
39. Cedeño-Caero, L.; Gomez-Bernal, H.; Fraustro-Cuevas, A.; Guerra-Gomez, H.D.; Cuevas-Garcia, R. Oxidative desulfurization of synthetic diesel using supported catalysts. Part III. Support effect on vanadium-based catalysts. *Catal. Today* **2008**, *133–135*, 244–254. [[CrossRef](#)]
40. Arellano, U.; Wang, Z.; Chen, L.; Wang, J.A.; Asomoza, M.; Estrella, A. VO_x core-shell catalysts for one-pot oxidation and separation of refractory multiaromatic sulfur compounds in a model diesel. *Ind. Eng. Chem. Res.* **2017**, *56*, 12080–12091. [[CrossRef](#)]
41. Wang, X.-J.; Li, F.-T.; Liu, J.-X.; Kou, C.-G.; Zhao, Y.; Hao, Y.-J.; Zhao, D. Preparation of TiO₂ in ionic liquid via microwave radiation and in situ photocatalytic oxidative desulfurization of diesel oil. *Energy Fuels* **2012**, *26*, 6777–6782. [[CrossRef](#)]
42. Li, L.; Zhang, J.; Shen, C.; Wang, Y.; Luo, G. Oxidative desulfurization of model fuels with pure nano-TiO₂ as catalyst directly without UV irradiation. *Fuel* **2016**, *167*, 9–16. [[CrossRef](#)]
43. Arellano, U.; Wang, J.; Timko, M.; Chen, L.; Carrera, S.P.; Asomoza, M.; González Vargas, O.; Llanos, M. Oxidative removal of dibenzothiophene in a biphasic system using sol-gel FeTiO₂ catalysts and H₂O₂ promoted with acetic acid. *Fuel* **2014**, *126*, 16–25. [[CrossRef](#)]

44. Fabián-Mijangos, L.; Cedeño-Caero, L. V loading effect on V₂O₅/ZrO₂ catalysts for oxidative desulfurization. *Ind. Eng. Chem. Res.* **2011**, *50*, 2659–2664. [[CrossRef](#)]
45. Gao, L.D.; Tang, Y.; Xue, Q.S.; Liu, Y.; Lu, Y. Hydrotalcite-like compounds derived CuZnAl oxide catalysts for aerobic oxidative removal of gasoline-range organosulfur compounds. *Energy Fuels* **2009**, *23*, 624–630. [[CrossRef](#)]
46. Yu, F.L.; Wang, R. Deep oxidative desulfurization of dibenzothiophene in simulated oil and real diesel using heteropolyan-on-substituted hydrotalcite-like compounds as catalysts. *Molecules* **2013**, *18*, 13691–13704. [[CrossRef](#)]
47. Timko, M.T.; Wang, J.A.; Burgess, J.; Kracke, P.; Gonzalez, L.; Jaye, C.; Fischer, D.A. Roles of surface chemistry and structural defects of activated carbons in the oxidative desulfurization of benzothiophenes. *Fuel* **2016**, *163*, 223–231. [[CrossRef](#)]
48. Arellano, U.; Shen, J.M.; Wang, J.A.; Timko, M.; Chen, L.; Vázquez Rodríguez, J.; Asomoza, M.; Estrella, A.; Gonzalez Vargas, O.; Llanos, M. Dibenzothiophene oxidation in a model diesel fuel using CuO/GC catalysts and H₂O₂ in the presence of acetic acid under acidic condition. *Fuel* **2015**, *149*, 15–25. [[CrossRef](#)]
49. Gonzalez, L.A.; Kracke, P.; Green, W.H.; Tester, J.W.; Shafer, L.M.; Timko, M.T. Oxidative desulfurization of middle-distillate fuels using activated carbon and power ultrasound. *Energy Fuels* **2012**, *26*, 5164–5176. [[CrossRef](#)]
50. Yang, G.; Zhang, X.; Yang, H.; Long, Y.; Ma, J. Sucrose facilitated synthesis of mesoporous silicoaluminophosphate SAPO-11 with different crystalline phases of MoO₃ for highly-efficient oxidative desulfurization. *J. Colloid Interface Sci.* **2018**, *532*, 92–102. [[CrossRef](#)]
51. Mirante, F.; Alves, A.C.; Juliãoa, D.; Almeida, P.L.; Gagoc, S.; Valençad, R.; Ribeiro, J.C.; de Castro, B.; Granadeiro, C.M.; Balula, S.S. Large-pore silica spheres as support for samarium-coordinated undecamolybdophosphate: Oxidative desulfurization of diesels. *Fuel* **2020**, *259*, 116213. [[CrossRef](#)]
52. Zhu, J.; Wu, P.; Chen, L.; He, J.; Wu, Y.; Wang, C.; Chao, Y.; Lu, L.; He, M.; Zhu, W.; et al. 3D-printing of integrated spheres as a superior support of phosphotungstic acid for deep oxidative desulfurization of fuel. *J. Energy Chem.* **2020**, *45*, 91–97. [[CrossRef](#)]
53. Akopyan, A.; Polikarpova, P.; Gul, O.; Anisimov, A.; Karakhanov, E. Catalysts based on acidic SBA-15 for deep oxidative desulfurization of model fuels. *Energy Fuels* **2020**, *34*, 14611–14619. [[CrossRef](#)]
54. Ekaterina, E.; Argkopyam, A.; Schepina, A.; Anna, I.S.; Aleksandrimov, A.; Mantximov, M.A. Deep aerobic oxidative desulfurization of model fuel by Anderson-type polyoxometalate catalysts. *Catal. Commun.* **2021**, *149*, 106256. [[CrossRef](#)]
55. Ramos, J.; Wang, J.; Flores, S.; Chen, L.; Nava, N.; Navarrete, J.; Domínguez, J.; Szpunar, J. Ultrasound-assisted synthesis and catalytic activity of mesostructured FeOx/SBA-15 and FeOx/Zr-SBA-15 catalysts for the oxidative desulfurization of model diesel. *Catal. Today* **2020**, *349*, 198–209. [[CrossRef](#)]
56. Parry, E.P. An infrared study of pyridine adsorbed on acidic solids. Characterization of surface acidity. *J. Catal.* **1963**, *2*, 371–379. [[CrossRef](#)]
57. Shylesh, S.; Singh, A.P. Vanadium-containing ordered mesoporous silicates: Does the silica source really affect the catalytic activity, structural stability, and nature of vanadium sites in V-MCM-41? *J. Catal.* **2005**, *233*, 359–371. [[CrossRef](#)]
58. Zhou, B.; He, D. Raman spectrum of vanadium pentoxide from density-functional perturbation theory. *J. Raman Spectrosc.* **2008**, *39*, 1475–1481. [[CrossRef](#)]
59. Baddour-Hadjean, R.; Smirnov, M.B.; Smirnov, K.S.; Kazimirov, V.Y.; Gallardo-Amores, J.M.; Amador, U.; Arroyo-de Dompablo, M.E.; Pereira-Ramos, J.P. Lattice dynamics of beta-V₂O₅: Raman spectroscopic insight into the atomistic structure of a high-pressure vanadium pentoxide polymorph. *Inorg. Chem.* **2012**, *51*, 3194–3201. [[CrossRef](#)] [[PubMed](#)]
60. Sáez, V.; Mason, T.J. Sono-electrochemical synthesis of nanoparticles. *Molecules* **2009**, *14*, 4284–4299. [[CrossRef](#)]
61. Kharisova, O.V.; Kharisov, B.I.; Ruíz Valdés, J.J.; Méndez, U.O. Ultrasound in nanochemistry: Recent advances. *Synth. React. Inorg. Met. Chem.* **2011**, *41*, 429–448. [[CrossRef](#)]
62. Rahimi, M.; Shahhosseini, S.; Sobati, M.A.; Movahedirad, S.; Khodaei, B.; Hassanzadeh, H. A novel multi-probe continuous flow ultrasound assisted oxidative desulfurization reactor; experimental investigation and simulation. *Ultrason. Sonochem.* **2019**, *56*, 264–273. [[CrossRef](#)]
63. Ugo, R.; James, B.R. Peroxometal complexes derived from hydrogen peroxide, some applications in organic synthesis. In *Catalytic Oxidations with Hydrogen Peroxide as Oxidant*; Metzler, J.B., Ed.; Springer: Dordrecht, The Netherlands, 1992; Volume 9, pp. 223–252.
64. De Filippis, P.; Scarsella, M.; Verdona, N. Peroxyformic acid formation: A kinetic study. *Ind. Eng. Chem. Res.* **2009**, *48*, 1372–1375. [[CrossRef](#)]
65. Arends, I.W.C.E.; Sheldon, R. Activities and stabilities of heterogeneous catalysts in selective liquid phase oxidations: Recent developments. *Appl. Catal. A Gen.* **2001**, *212*, 175–187. [[CrossRef](#)]
66. Wei, S.; He, H.; Cheng, Y.; Yang, C.; Zeng, G.; Qiu, L. Performances, kinetics and mechanisms of catalytic oxidative desulfurization from oils. *RSC Adv.* **2016**, *6*, 103253–103269. [[CrossRef](#)]
67. Chong, C.C.; Teh, L.P.; Setiabudi, H.D. Syngas production via CO₂ reforming of CH₄ over Ni-based SBA-15: Promotional effect of promoters (Ce, Mg, and Zr). *Mater. Today Energy* **2019**, *12*, 408–417. [[CrossRef](#)]
68. Kongwudthiti, S.; Praserttham, P.; Tanakulrungsank, W.; Inoue, M. The influence of Si–O–Zr bonds on the crystal-growth inhibition of zirconia prepared by the glycothermal method. *J. Mater. Process. Technol.* **2003**, *136*, 186–189. [[CrossRef](#)]

-
69. Jiang, W.; Zheng, D.; Xun, S.; Qin, Y.; Lu, Q.; Zhu, W.; Li, H. Polyoxometalate-based ionic liquid supported on graphite carbon induced solvent-free ultra-deep oxidative desulfurization of model fuels. *Fuel* **2017**, *190*, 1–9. [[CrossRef](#)]
 70. D'Anna, F.; Grilli, M.L.; Petrucci, R.; Feroci, M. WO₃ and ionic liquids: A synergic pair for pollutant gas sensing and desulfurization. *Metals* **2020**, *10*, 475. [[CrossRef](#)]